



This is the accepted manuscript made available via CHORUS. The article has been published as:

Element orbitals for Kohn-Sham density functional theory

Lin Lin and Lexing Ying

Phys. Rev. B **85**, 235144 — Published 25 June 2012

DOI: [10.1103/PhysRevB.85.235144](https://doi.org/10.1103/PhysRevB.85.235144)

Element orbitals for Kohn-Sham density functional theory

Lin Lin^{1,*} and Lexing Ying²

¹*Computational Research Division, Lawrence Berkeley National Laboratory, Berkeley, CA 94720, USA*

²*Department of Mathematics and ICES, University of Texas at Austin, Austin, TX 78712, USA*

We present a method to discretize the Kohn-Sham Hamiltonian matrix in the pseudopotential framework by a small set of basis functions automatically contracted from a uniform basis set such as planewaves. Each basis function is localized around an element, which is a small part of the global domain containing multiple atoms. We demonstrate that the resulting basis set achieves meV accuracy for 3D densely packed systems with a small number of basis functions per atom. The procedure is applicable to both insulating and metallic systems.

PACS numbers: 71.15.Ap, 71.15.Nc

I. INTRODUCTION

Kohn-Sham density functional theory (KSDF) is the most widely used electronic structure theory for condensed matter systems. When solving the Kohn-Sham equations, the choice of basis functions usually poses a dilemma for practitioners. The accurate and systematically improvable basis functions that are uniform in space, such as plane waves or finite elements, typically result in a large number of degrees of freedom (500 ~ 10000) per atom in the framework of norm conserving pseudopotential² especially for transition metal elements. The number of basis functions per atom can be reduced to the order of hundreds using ultrasoft pseudopotential³, or augmentation techniques in the core-region such as the linearized augmented plane-wave (LAPW) method⁴ and the projector augmented wave (PAW) method⁵. The relatively large number of basis functions used leads to a large prefactor in front of the already expensive cubic scaling for solving KSDF.

Contracted basis functions, such as Gaussian type orbitals, atomic orbitals or muffin-tin orbitals, can represent the Kohn-Sham orbitals with a small number of degrees of freedom per atom (4 ~ 100). These contracted basis functions contain a number of parameters to be determined. The flexibility for choosing different forms of parameters has generated a vast amount of literature (see *e.g.* Refs. 6–11) in the past few decades, which has been reviewed recently in Ref. 12. Compared to the uniform basis set in which the accuracy is controlled by a few universal parameters such as the planewave cutoff or the grid spacing, the parameters in the contracted basis functions are typically constructed by a fitting procedure for a range of reference systems. The fitting procedure as well as the reference systems should be carefully chosen in order to obtain accurate results with a small number of degrees of freedom.

It is desirable to combine the advantage of uniform basis functions in which the accuracy is controlled by no more than a handful of universal parameters for almost all materials, and the advantage of contracted basis functions with a very small number of basis functions per atom. In other words, we would like to generate a small

number of contracted basis functions by a unified procedure with high accuracy comparable to that obtained from uniform basis functions. In a recent work¹³, we have developed a unified method for constructing a set of contracted basis functions from a uniform basis set such as planewaves in the pseudopotential framework. The new basis set, called the adaptive local basis (ALB) set, is constructed by solving the Kohn-Sham problem restricted to a small part of the domain called *element*. Each ALB is discontinuous from the perspective of the global domain, and the continuous Kohn-Sham orbitals are approximated by the discontinuous ALBs under a discontinuous Galerkin framework¹⁴. It was demonstrated that the ALBs are able to achieve high accuracy (in the order of 1 meV) using disordered Na and Si as examples. However, the number of basis functions per atom increases with respect to dimensionality. For example, 40 basis functions per atom is needed to reach the accuracy of 1 meV/atom for 3D bulk Na system.

In this paper, we propose a new basis set that is constructed from linear combination of adaptive local basis functions. Each new basis function, dubbed *element orbital* (EO), has localized nature around its associated element of the domain. The number of EOs used is significantly reduced compared to the number of ALBs for 3D bulk systems. We demonstrate that 4 EOs per atom are sufficient to achieve 1 meV per atom accuracy for 3D bulk Na system with disorderedness. We also apply EOs to study Na, Si and graphene, with varying system sizes, lattice constants or types of defects. The new method consistently achieves meV accuracy for calculating the total energy when compared to standard electronic structure software such as ABINIT¹⁵. Since the EOs are contracted from a uniform basis set such as planewave basis set, the shape of the EOs has more flexibility to reflect the environmental effect than contracted basis sets which are centered around atoms. Numerical result indicates that the shape of EOs can resemble both atomic orbitals of different angular momentum and chemical bonds centered in the interstitial region, depending on their chemical environment.

We remark that the construction of the EOs is closely related to several existing techniques for reducing the

number of basis functions per atom, starting from a large primitive basis set consisting of Gaussian orbitals or atomic orbitals^{6,7,16,17}. However, the EOs are contracted from a fine uniform basis set such as planewaves, and a number of difficulties arise to make it difficult for the previous techniques to be applied directly. For instance, the filtration technique in Ref. 16,17 constructs a near-minimal basis set from a large number of Gaussian type orbitals by applying a filtration matrix to a set of trial orbitals, taken from one or a few Gaussian-type orbitals. When the Gaussian-type orbitals are replaced by a fine uniform basis set such as planewaves, finding a good set of trial orbitals itself becomes a difficult task, and the construction of trial orbitals can inevitably introduce a set of undetermined parameters, which is not desirable in the current framework.

This paper is organized as follows: Section II introduces the adaptive local basis functions in the discontinuous Galerkin framework for solving Kohn-Sham density functional theory in the pseudopotential framework. The construction of the element orbitals is introduced in Section III. Section IV discusses briefly the implementation procedure of element orbitals. The performance of element orbitals is reported in Section V, followed by the discussion and conclusion in Section VI.

II. ADAPTIVE LOCAL BASIS FUNCTIONS

Consider a quantum system with N electrons under external potential by V_{ext} in a rectangular domain Ω with periodic boundary condition. To simplify the equations, we ignore the electron spin for now. In Kohn-Sham density functional theory at a finite temperature $T = 1/(k_B\beta)^{1,18}$, the Helmholtz free energy is given by

$$\begin{aligned} \mathcal{F}_{\text{tot}} = \mathcal{F}_{\text{tot}}(\{\psi_i\}, \{f_i\}) = & \frac{1}{2} \sum_i f_i \int |\nabla \psi_i(x)|^2 dx \\ & + \int V_{\text{ext}}(x) \rho(x) dx + \sum_\ell \gamma_\ell \sum_i f_i \left| \int b_\ell^*(x) \psi_i(x) dx \right|^2 \\ & + \frac{1}{2} \iint \frac{\rho(x)\rho(y)}{|x-y|} dx dy + \int \epsilon_{\text{xc}}[\rho(x)] dx \\ & + \beta^{-1} \sum_i (f_i \ln f_i + (1-f_i) \ln(1-f_i)), \quad (1) \end{aligned}$$

Correspondingly $\{\psi_i(x)\}$ and $\{f_i\}$ are the solutions to the minimization problem

$$\begin{aligned} \min_{\{\psi_i\}, \{f_i\}} \mathcal{F}_{\text{tot}}(\{\psi_i\}, \{f_i\}), \\ \text{s.t.} \quad \int \psi_i^*(x) \psi_j(x) dx = \delta_{ij}, \quad i, j = 1, \dots, \tilde{N}. \end{aligned} \quad (2)$$

$\{f_i\} \in [0, 1]$ are the occupation numbers which add up to the total number of electrons $N = \sum_{i=1}^{\tilde{N}} f_i$. Here we use exchange-correlation functional under local density approximation (LDA)^{19,20} and adopt norm conserving

pseudopotential², with the projection vector of the non-local pseudopotential in the Kleinman-Bylander form²¹ denoted by $\{b_\ell(x)\}$, and $\gamma_\ell = \pm 1$ is a sign. The number of eigenstates \tilde{N} calculated in practice is chosen to be slightly larger than the number of electrons N in order to compensate for the finite temperature effect, following the criterion that the occupation number $f_{\tilde{N}}$ is sufficiently small (less than 10^{-8}). The electron density is given by

$$\rho(x) = \sum_{i=1}^{\tilde{N}} f_i |\psi_i(x)|^2.$$

The Kohn-Sham equation, or the Euler-Lagrange equation associated with (2) is^{1,18}

$$H[\rho]\psi_i = \left(-\frac{1}{2}\Delta + V_{\text{eff}}[\rho] + \sum_\ell \gamma_\ell |b_\ell\rangle\langle b_\ell|\right)\psi_i = \lambda_i \psi_i, \quad (3)$$

where the effective one-body potential $V_{\text{eff}}[\rho]$ is

$$V_{\text{eff}}[\rho](x) = V_{\text{ext}}(x) + \int \frac{\rho(y)}{|x-y|} dy + \epsilon'_{\text{xc}}[\rho(x)]$$

and the occupation numbers $\{f_i\}_{i \geq 1}$ follow the Fermi-Dirac distribution

$$f_i = \frac{1}{1 + \exp(\beta(\lambda_i - \mu))}.$$

Here the chemical potential μ is chosen so that $\sum_{i=1}^{\tilde{N}} f_i = N$. In each SCF iteration of (3), we freeze ρ and solve for the \tilde{N} lowest eigenfunctions $\{\psi_i(x)\}_{1 \leq i \leq \tilde{N}}$. This linear eigenvalue problem is the focus of the following discussion.

The discontinuous Galerkin (DG) framework¹⁴ provides flexibility in choosing appropriate basis functions to discretize the Kohn-Sham Hamiltonian $H[\rho]$. In the DG framework, a smooth function delocalized across the global domain can be systematically approximated by a set of discontinuous functions that are localized in the real space. Let $\mathcal{T} = \{E_1, E_2, \dots, E_M\}$ be a collection of *elements*, i.e. disjoint rectangular partitions of Ω , and \mathcal{S} be the collection of surfaces $\{\partial E_k\}$ that correspond to each element E_k in \mathcal{T} . We associate with each E_k a set of orthogonal basis functions $\{u_{k,j}(x)\}_{1 \leq j \leq J_k}$ supported in E_k , with the total number of basis functions given by

$$N^b = \sum_{k=1}^M J_k.$$

Under such a basis set, the Hamiltonian is discretized

into an $N^b \times N^b$ matrix with entries given by

$$\begin{aligned}
 & H(k', j'; k, j) \\
 &= \frac{1}{2} \langle \nabla u_{k', j'}, \nabla u_{k, j} \rangle_{\mathcal{T}} - \frac{1}{2} \langle [[u_{k', j'}]], \{ \{ \nabla u_{k, j} \} \} \rangle_{\mathcal{S}} \\
 & - \frac{1}{2} \langle \{ \{ \nabla u_{k', j'} \} \}, [[u_{k, j}]] \rangle_{\mathcal{S}} + \alpha \langle [[u_{k', j'}]], [[u_{k, j}]] \rangle_{\mathcal{S}} \\
 & + \langle u_{k', j'}, V_{\text{eff}} u_{k, j} \rangle_{\mathcal{T}} + \sum_{\ell} \gamma_{\ell} \langle u_{k', j'}, b_{\ell} \rangle_{\mathcal{T}} \langle b_{\ell}, u_{k, j} \rangle_{\mathcal{T}},
 \end{aligned} \tag{4}$$

where $\langle \cdot, \cdot \rangle_{\mathcal{T}}$ and $\langle \cdot, \cdot \rangle_{\mathcal{S}}$ are inner products in the bulk and on the surface respectively, and $\alpha > 0$ is a fixed parameter for penalizing cross-element discontinuity. The notations $\{ \{ \cdot \} \}$ and $[[\cdot]]$ stand for the average and jump operators across surfaces¹⁴. Comparing (3) and (4), the new terms involving the average and jump operators can be derived from integration by parts of the Laplacian operator, and provide consistency and stability of the DG method²².

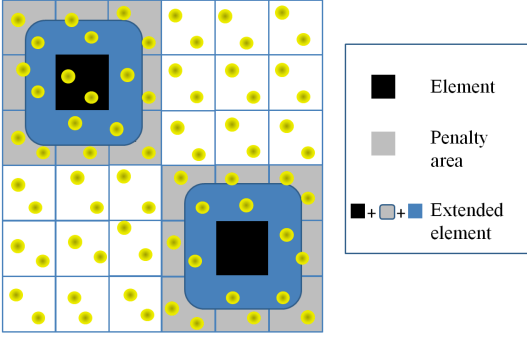


FIG. 1: (color online) Sketch for the construction of adaptive local basis functions and element orbitals. Each adaptive local basis function is supported in an element. Each element orbital is supported in an extended element.

In the work of adaptive local basis set¹³, the functions $\{u_{k, j}\}_{1 \leq j \leq J_k}$ in each element E_k are determined as follows. Let d be the dimension of the system. For each E_k (one black box in Fig. 1), we define an associated extended element Q_k , which includes both E_k and its $3^d - 1$ neighboring elements. Define $H_{Q_k}[\rho]$ to be the restriction of $H[\rho]$ to Q_k with periodic boundary condition and with potential given by the restriction of $V_{\text{eff}}[\rho]$ to Q_k . $H_{Q_k}[\rho]$ is then discretized and diagonalized with uniform basis functions such as plane waves. We denote the corresponding eigenvalues and eigenfunctions by $\{\lambda_{k, j}\}_{j \geq 1}$ and $\{\varphi_{k, j}(x)\}_{j \geq 1}$, respectively, starting from the lowest eigenvalue. One then restricts the first J_k functions of $\{\varphi_{k, j}(x)\}_{j \geq 1}$ to E_k , where J_k is set to be proportional to the number of electrons inside the extended element Q_k (see the numerical examples for specific choice of J_k). In addition, we define for each E_k

$$\lambda_k^c = \lambda_{k, J_k}, \tag{5}$$

i.e. the largest selected eigenvalue in E_k which shall be used later. Applying the Gram-Schmidt procedure to $\{\varphi_{k, j}(x)\}_{1 \leq j \leq J_k}$ then gives rise to a set of orthonormal functions

$$\{u_{k, j}(x)\}_{1 \leq j \leq J_k} \tag{6}$$

for each E_k . The union of such functions over all elements $\{u_{k, j}(x)\}_{1 \leq k \leq M, 1 \leq j \leq J_k}$ gives the set of adaptive local basis functions (ALBs).

For a given system, the partition of E_k is kept to be the same even with changing atomic configurations as in the case of structure optimization and molecular dynamics. Dangling bonds may form when atoms are present on the surface of the extended elements, but we emphasize that these dangling bonds are not needed to be passivated by introducing auxiliary atoms near the surface of the extended elements²³. This is because the potential is not obtained self-consistently within Q_k , but instead from the restriction of the screened potential in the global domain Ω to Q_k in each SCF iteration, which mutes the catastrophic damage of the dangling bonds. The oscillation in the basis functions caused by the discontinuity of the potential at the surface of the Q_k (called Gibbs phenomenon) still exists, but it damps exponentially away from the surface of Q_k and has controlled effect in E_k . Using disordered Na and Si as examples, we demonstrated that ALB can achieve meV accuracy per atom using 4 ~ 40 basis functions per atom¹³.

III. ELEMENT ORBITALS

The high accuracy of ALBs indicates that the span of $\{u_{k, j}\}_{1 \leq k \leq M, 1 \leq j \leq J_k}$ approximately contains the span of the Kohn-Sham orbitals $\{\psi_i\}_{1 \leq i \leq \tilde{N}}$. However, we found that the number of basis functions per atom may vary significantly with respect to the dimensionality d of the system, which has not been seen reported in the literature using traditional contracted basis set to the extent of our knowledge.

The dimension dependence of ALBs can be intuitively understood as follows, motivated from the success of the contracted basis set such as atomic orbitals. Consider the case where an atom is positioned at the center of element E_k and assume for simplicity that each of its atomic orbital overlaps only with the neighboring elements (i.e., those inside the extended element Q_k). In order to include one atomic orbital, denoted by $\eta(x)$, in the span of $\{u_{k, j}(x)\}_{1 \leq k \leq M, 1 \leq j \leq J_k}$, each neighboring element $E_{k'}$ in Q_k should allocate one of its ALBs to represent the restriction of $\eta(x)$ in $E_{k'}$. This implies that N^b , the total number of ALBs, should roughly be equal to $3^d \tilde{N}$, which becomes increasingly redundant with respect to the dimension d . In fact, this is close to what has been observed in the numerical experiments¹³.

In order to avoid this redundancy and motivated by the construction of atomic orbitals, we propose to build

a new basis set by piecing the ALBs in neighboring elements $\{E_{k'}\}$ in Q_k to construct functions that are qualitatively close to the atomic orbitals. To distinguish them from the pre-fitted atomic orbitals, we name these functions *element orbitals* (EOs). In order to construct them, one is faced mainly with three issues. First, the ALBs are always discontinuous across the element boundaries, while qualitatively the EOs should be a *continuous* function since the atomic orbitals are continuous. Second, when one pieces back the ALBs to obtain the EOs, it is essential that the resulting functions have *low-energy*. Finally, one needs to make sure that the EOs of element E_k should be *localized* at E_k in order to avoid potential linear dependence among the EOs of different elements.

A two-step procedure is proposed to address these three issues. In the first step, we construct, for each element E_k , a set of *candidate functions* that take care of the first two issues. Then in the second step, the element orbitals are identified by localizing the candidate functions. More specifically, the method proceeds as follows.

Let us fix an element E_k . First, since each ALB is only supported in its associated element and equal to zero outside, we seek for a set of *candidate functions* of element E_k that are linear combinations of the ALBs of both E_k and its $3^d - 1$ neighbors (Fig. 1). Denoting by \mathcal{I} the index of all the ALBs, and by $\mathcal{I}_k \subset \mathcal{I}$ the index set of ALBs supported in Q_k , we define a local Hamiltonian

$$H_k = H(\mathcal{I}_k, \mathcal{I}_k),$$

i.e., the restriction of H to the index set \mathcal{I}_k . Following the intuition that the atomic orbitals should only be affected by the local environment of E_k , it is reasonable to assume that the low eigenfunctions of H_k serve as good candidate functions. Computationally, we diagonalize H_k by

$$H_k M_k = M_k \Delta_k, \quad (7)$$

where the diagonal of Δ_k contains all the eigenvalues bounded from above by the cut-off energy λ_k^c given by (5) and the columns of M_k contains the corresponding eigenfunctions. The matrix M_k is called the *merging matrix* of element E_k . We argue that this step addresses the continuity and low-energy issues of the element orbitals, since the eigenfunctions in (7) are qualitatively smooth due to the cross-element penalty term of the DG formulation and choosing the eigenfunctions below λ_k^c also ensures that the candidate functions have low-energy.

Second, we localize these candidate functions to be centered at E_k using a penalizing weight function $w_k(x)$ defined for $x \in Q_k$. $w_k(x)$ is only nonzero in the extended element Q_k outside a certain distance, called the *localization radius*, from the boundary of E_k (light gray area in Fig. 1). For simplicity we choose $w_k(x) = 1$ in the penalty area and 0 otherwise. More sophisticated weighting function and confining potentials (as developed for linear scaling methods²⁴ and for atomic orbitals⁸) can be used and optimized for EOs in the future work. A weighting matrix W_k for the adaptive basis functions in

the index set \mathcal{I}_k is defined in the extended element Q_k by

$$W_k(k', j'; k'', j'') = \langle u_{k', j'}, w_k \cdot u_{k'', j''} \rangle_{\mathcal{T}}.$$

In order to localize the candidate functions, we solve a second eigenvalue problem

$$(M_k^t W_k M_k) L_k = M_k^t M_k L_k \Gamma_k = L_k \Gamma_k, \quad (8)$$

where $M_k^t M_k = \mathcal{I}$ since M_k is orthonormal from (7). The columns of L_k and the diagonal of Γ_k consist of the first N_k^o eigenfunctions and eigenvalues, respectively. Here N_k^o is the number of element orbitals (EOs) of E_k . As will be shown later in the numerical results, a small number of EOs per atom already achieve high accuracy in the total energy calculation. We call the matrix L_k the *localization matrix*, and the product $M_k L_k$ gives the coefficients of the EOs in E_k in terms of the ALBs indexed by \mathcal{I}_k . In order to present these EOs in terms of the whole adaptive basis set, we introduce for E_k an $|\mathcal{I}| \times |\mathcal{I}_k|$ *selection matrix* S_k such that $S_k(\mathcal{I}_k, \mathcal{I}_k)$ is equal to the identity and all zero otherwise. By defining the $N^b \times N_k^o$ coefficient matrix $C_k = S_k M_k L_k$, we can construct the element orbitals associated with E_k by

$$\phi_{k,l}(x) = \sum_{k', j'} u_{k', j'}(x) (C_k)_{k' j'; l}, \quad l = 1, \dots, N_k^o. \quad (9)$$

Note that, since these functions are localized in the extended element Q_k by construction, the index k' only runs through the elements inside Q_k . Finally, the coefficient matrix

$$C = (C_1, \dots, C_M)$$

gives the whole set of coefficients of the $N^o = \sum_{k=1}^M N_k^o$ EOs in terms of the adaptive local basis functions (ALBs). Once the EOs are identified, we solve an $N^o \times N^o$ generalized eigenvalue problem

$$(C^t H C) V = (C^t C) V \Lambda, \quad (10)$$

where the diagonal of Λ gives the Kohn-Sham eigenvalues $\{\lambda_i\}_{1 \leq i \leq \tilde{N}}$ and the columns of V provide the coefficients of the Kohn-Sham orbitals in terms of the EOs. From $\{\lambda_i\}_{1 \leq i \leq \tilde{N}}$, one can calculate the chemical potential μ and the occupation number $\{f_i\}_{1 \leq i \leq \tilde{N}}$. Finally, by introducing the Gram matrix

$$G = C V \cdot \text{diag}(f_i) \cdot (C V)^t,$$

we can write $\rho(x)$ as

$$\rho(x) = \sum_{j', j''} u_{k(x), j'}(x) \cdot G(k(x), j'; k(x), j'') \cdot u_{k(x), j''}(x), \quad (11)$$

where $k(x)$ indexes the element that contains x . Solving the generalized eigenvalue problem (10) is a cubic scaling procedure. However, notice that one only needs the knowledge of the diagonal blocks of the Gram matrix G to

construct the electron density. This allows us to use the recently developed pole expansion and selected inversion type fast algorithms^{25–30} to reduce the asymptotic scaling for solving the generalized eigenvalue problem (10) from cubic scaling to at most quadratic scaling for 3D bulk systems. For simplicity we employ a cubic scaling implementation within the current work, as described in more detail in Section IV.

IV. PARALLEL IMPLEMENTATION

Our algorithm is implemented fully in parallel for message-passing environment, based on the implementation details presented in Ref. 13. Here we summarize the key components of the parallel implementation.

The global domain is discretized with a uniform Cartesian grid with a spacing fine enough to capture the local oscillations of the Kohn-Sham orbitals and the electron density. Rather than using the dual grid approach with one set of grid for representing the Kohn-Sham wavefunctions, and another set of denser grid for representing the electron density, we only use one set of Cartesian grid for both the Kohn-Sham wavefunctions and the electron density for simplicity of the implementation. The grid inside an element E_k is a three-dimensional Cartesian Legendre-Gauss-Lobatto (LGL) grid in order to accurately carry out the operations of the basis functions such as numerical integration. The ALBs are first represented in a planewave basis set in each extended element Q_k solved by LOBPCG algorithm³¹ with a preconditioner³², and are interpolated to each element E_k and orthogonalized. The eigenvalue problems involved in constructing the EOs are performed by LAPACK subroutine `dsyevd`.

To simplify the discussion of the parallel implementation, we assume that the number of processors is equal to the number of elements. It is then convenient to index the processors $\{P_k\}$ with the same index k used for the elements. In the more general setting where the number of elements is larger than the number of processors, each processor takes a couple of elements and the following discussion will apply with only minor modification. Each processor P_k locally generates and stores the ALBs $\{u_{k,j}(x)\}$ for $j = 1, 2, \dots, J_k$ and the coefficients for the EOs $\{(C_k)_{k',j';l}\}$ for k' running through the elements in Q_k , $j' = 1, 2, \dots, J_{k'}$ and $l = 1, 2, \dots, N_k^o$. The EOs $\{\phi_{k,l}(x)\}$ are not explicitly formed in the real space. We further partition the non-local pseudopotentials $\{b_\ell(x)\}$ by assigning $b_\ell(x)$ to the processor P_k if and only if the atom associated to $b_\ell(x)$ is located in the element E_k .

Since the matrices C and H are sparse, the Hamiltonian matrix $C^t H C$ and the mass matrix $C^t C$ in (10) are also sparse matrices. However, these matrices are treated as dense matrices in our implementation for simplicity. The parallel matrix-matrix multiplication for constructing $C^t H C$ and $C^t C$ are performed using PBLAS subroutine `pdgemm`, and the generalized eigenvalue problem (10) is solved by converting it to a standard eigen-

value problem using ScaLAPACK³³ subroutine `pdpotrf` and `pdsygst`, and the standard eigenvalue problem is solved by ScaLAPACK subroutine `pdsyevd`.

In our implementation, the matrices H and C are constructed locally according to the element indices. However, the ScaLAPACK routines that operate on H and C require them to be stored in the two dimensional block cyclic pattern. In order to support these two types of data storage, we have implemented a rather general communication framework that only requires the programmer to specify the desired non-local data. This framework then automatically fetches the data from the processors that store them locally. The actual communication is mostly done using asynchronous communication routines `MPI_Isend` and `MPI_Irecv`.

V. NUMERICAL RESULTS

The new method is implemented with Hartwigsen-Goedecker-Hutter (HGH) pseudopotential³⁴, with the local and nonlocal pseudopotential implemented fully in the real space³⁵. Finite temperature formulation of the Kohn-Sham density functional theory¹⁸ is used, and the temperature is set to be 2000K only for the purpose of accelerating the convergence of SCF iteration. Since finite temperature is used, the accuracy is quantified by the error of the total free energy³⁶ per atom. HGH pseudopotential has analytic expression, which allows us to minimize the effect of numerical interpolation and to perform accurate comparison with existing electronic structure code. We compare our result with ABINIT¹⁵ which also supports the HGH pseudopotential. The ALBs and EOs start from random initial guess, and are refined iteratively in the SCF iteration together with the electron density. In all the calculations, Anderson mixing³⁷ with Kerker preconditioner³⁸ is used for the SCF iteration. Gamma point Brillouin sampling is used for simplicity for all calculations. In Section II and Section III, we count the number of basis functions in terms of the number of ALBs per element and the number of EOs per element. In this section, we count the number of ALBs and EOs per atom instead, in order to be consistent with literature. All computational experiments are performed on the Hopper system at the National Energy Research Scientific Computing (NERSC) center. Each Hopper node consists of two twelve-core AMD “MagnyCours” 2.1-GHz processors and has 32 gigabytes (GB) DDR3 1333-MHz memory. Each core processor has 64 kilobytes (KB) L1 cache and 512KB L2 cache. It also has access to a 6 megabytes (MB) of L3 cache shared among 6 cores.

As mentioned earlier, the ALBs have been shown to achieve effective dimension reduction for quasi-1D systems, but with deteriorating performance as the dimensionality of the system increases¹³. Using Na as example, it has been shown that while 4 ALBs per atom is enough to reach 1 meV accuracy for quasi-1D systems, 40 ALBs per atom is necessary to reach the same accuracy for 3D

bulk systems. Now using a 3D bulk Na system with 432 atoms as example, we illustrate that the number of basis functions per atom can be effectively reduced using EO.

The supercell for Na is simple cubic and the length of the supercell along each dimension is 45.6 a.u.. A random perturbation with standard deviation 0.2 a.u. is applied to each atom in the supercell to eliminate the translational invariance of the system. The supercell is partitioned into $6 \times 6 \times 6$ elements, with the length of each dimension of each element being 7.6 a.u.. The length of each dimension of each extended element is 22.8 a.u. which is 3 times larger than that of the element. The penalty parameter α in (4) is set to be 100. The supercell is discretized with a uniform mesh of dimension $120 \times 120 \times 120$ in the real space. This mesh is used for representing both the electron density and the Kohn-Sham orbitals, which corresponds to a planewave cut-off of 68 Ry in the Fourier space. ABINIT uses a dual grid for representing the Kohn-Sham wavefunctions and the electron density. The planewave cutoff for wavefunctions used in ABINIT is 20 Ry. This corresponds to a planewave cutoff for the electron density at 80 Ry, with a uniform mesh of dimension $135 \times 144 \times 144$ in the real space. The different numbers of grid points along each dimension come from the automatic grid adjustment in ABINIT. We remark that the grid size is chosen to be larger than the typical setup in electronic calculation for Na to make sure that the error introduced by the grid size is small compared to that introduced by using ALBs and EOs. Inside each element a Legendre-Gauss-Lobatto (LGL) grid of dimension $30 \times 30 \times 30$ is used for numerical integration in the assembly process of the discretized Hamiltonian matrix H . The error of the total free energy per atom only using ALBs is shown in Fig. 2 (a). The error systematically decreases with the increase of the number of ALBs. When the number of ALBs exceeds 35, the error of the total free energy per atom is less than 1 meV.

Element orbitals (EOs) provide further dimension reduction compared to ALBs. Fig. 2 (b) shows the difference of the free energy per atom calculated from EOs and that from ABINIT. We construct EOs from as many as 42 ALBs per atom, following the criterion (5) for the choice of the candidate functions and using a localization radius of 6.0 a.u.. Compared to a converged ALB calculation, the error using only 3 EOs per atom is already within 5 meV per atom. When 6 EOs are used, the total free energy calculated is essentially the same as that using 42 ALBs, and the error compared to ABINIT is less than 1 meV per atom. Fig. 2 (b) indicates that the EOs are indeed effective for reducing the number of basis functions per atom for 3D bulk systems.

Compared to ALB, the EO approach introduces an additional parameter which is the localization radius. Fig. 2 (c) shows the error of the total free energy per atom using 42 ALBs per atom, and 6 EOs per atom but with different localization radius. When the localization radius is 4.0 a.u. which is 53% the length of an element, the error

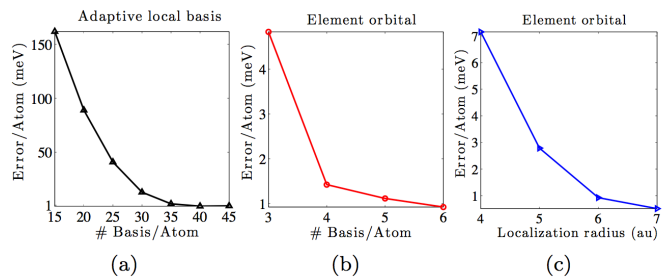


FIG. 2: (color online) (a) Convergence of adaptive local basis functions (ALB) for a 3D bulk Na system with 432 atoms. (b) Convergence of element orbitals (EO) for the same Na system with fixed number of ALBs. (c) Convergence in terms of the localization radius for the same Na system with fixed number of ALBs and fixed number of EOs.

of the total energy per atom is 7 meV. Moderate choice of the localization radius of 6.0 a.u. (69% of the length of an element) yields accuracy around 1 meV per atom. Fig. 2 (c) shows that our method is stable even for a large localization radius 7.0 a.u. (92% of the length of an element), and the error is even smaller and is below 1 meV per atom. We also remark that if the localization radius is further increased, the EOs are no longer localized around the element, but become fully extended in the extended element. This can lead to an unstable scheme with large error. Numerical experience indicates that setting the localization radius to be 60% ~ 90% of the length of the element provides good compromise between accuracy and stability in practice. Fig. 2 (c) shows that the accuracy of the EO is not very sensitive to the choice of localization radius.

EOs can resemble atomic orbitals but with local modifications reflecting the environmental effect, despite the fact that they are constructed in the extended elements with rectangular domain. Using the same Na system as example, we show in Fig. 3 the isosurface of the first 9 element orbitals (ϕ_1 to ϕ_9) belonging to the same extended element, with the red and blue color indicating the positive and negative part of the EOs, respectively. 27 atoms nearest to these EOs within a sphere of radius 6.0 a.u. are also plotted in Fig. 3 as gold balls. We see that ϕ_1 mimics s orbital, ϕ_2 - ϕ_4 mimic p -orbitals, and ϕ_5 - ϕ_9 mimic d -orbitals. Both the general shape and the multiplicity of the element orbitals agree well with the physical intuition. We also find that hybridization of the s , p , d orbitals naturally appears in the EOs, reflecting the effect of the environment. For example, the isosurface of ϕ_1 exhibits “holes” around atoms. These holes are not described in the spherical symmetric s atomic orbital, but can only be reflected in orbitals of higher angular momentum such as d orbitals. Therefore, EOs are natural generalization of atom-centered orbitals, with both the atomic and environmental effect taken into account

simultaneously.

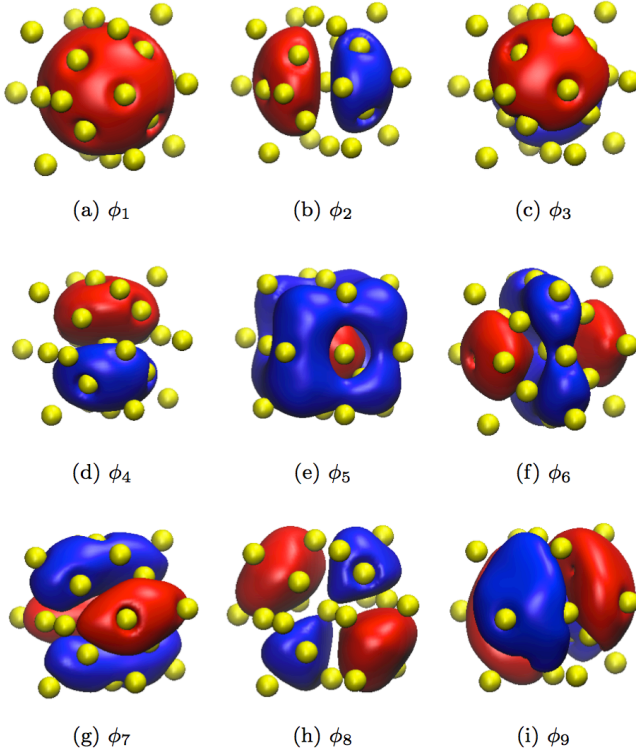


FIG. 3: The isosurface of the first 9 element orbitals belonging to the same extended element, for a 3D disordered bulk Na system in a supercell with 432 atoms. The 27 Na atoms nearest to the element orbitals within a sphere of radius 6.0 a.u. are plotted as gold balls. The positive and negative part of the element orbitals are represented by red and blue color, respectively.

EOs are localized in the extended elements. Since each candidate function is not continuous across the boundary of the extended element, EOs are still discontinuous across the boundary of the extended element. Nonetheless, the EOs are “qualitatively continuous” at the boundary of the extended elements. Fig. 4 (a) shows the behavior of ϕ_1, ϕ_4, ϕ_7 for the Na system along one [100] direction, with the zoom-in near the boundary of the extended element shown in Fig. 4 (b). EOs are very close to a continuous function especially for ϕ_1 and ϕ_4 with lower angular momentum. The value of EOs of higher angular momentum such as ϕ_7 at the grid point closest to the boundary of the extended element is within 10^{-3} .

EOs can be used for calculating the relative energies of different atomic configurations. Fig. 5 (a) shows the total free energy per atom for a crystal of Na consisting of $6 \times 6 \times 6 = 216$ unit cells with 432 atoms. Each unit cell is body centered cubic with 2 Na atoms. The lattice constant ranges from 7.3 a.u. to 7.9 a.u.. The size of each

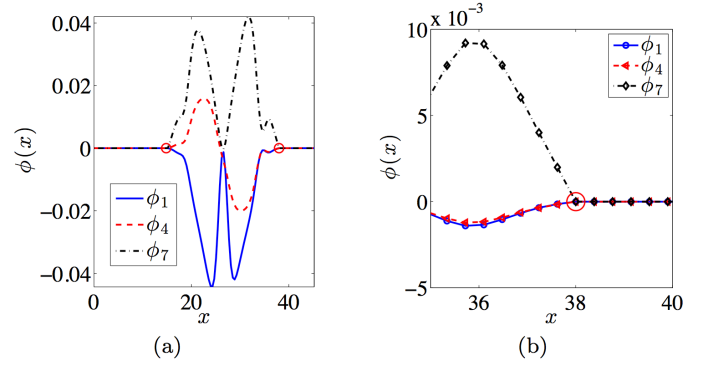


FIG. 4: (color online) (a) The value of the element orbitals ϕ_1 (blue solid line), ϕ_4 (red dashed line), and ϕ_7 (black dot dashed line) along one [100] direction of a 3D disordered bulk Na system with 432 atoms. The two red circles indicate the boundary of the extended element. (b) Zoom-in of (a) to the region near the boundary of the extended element. The same set of element orbitals ϕ_1 (blue solid line with circles), ϕ_4 (red dashed line with triangles) and ϕ_7 (black dot dashed line with diamonds) are shown, with the symbols indicating the position of the numerical grids. The red circle indicates the boundary of the extended element.

element is equal to that of one unit cell. 4 EOs per atom are constructed from 42 ALBs per atom and are used for calculating the total free energy. The planewave cutoff for Kohn-Sham wavefunctions in ABINIT is 20 Ry. The difference of the total energy per atom is less than 2 meV across all the lattice constants. Similar result can be obtained for Si. The supercell for Si contains $4 \times 4 \times 4 = 64$ unit cells with 512 atoms in total. Each unit cell is diamond cubic with 8 Si atoms. Fig. 5 (b) reports the total free energy per atom for lattice constants from 9.9 a.u. to 10.5 a.u.. Each element only covers $\frac{2}{3} \times \frac{2}{3} \times \frac{2}{3}$ unit cells. We remark that elements occupying a fraction of the unit cell are allowed, which is important especially when EOs are applied to systems with defects and disorderedness. The planewave cutoff for Kohn-Sham wavefunctions in ABINIT is set to be 120 Ry to achieve the high accuracy as benchmark solution. The localization radius is also 6.0 a.u.. Starting from 50 ALBs per atom, 10 EOs per atom are computed. The difference of the total free energy per atom is less than 1 meV for all lattice constants.

EOs are also effective for calculating the total energy of systems with defects. For a crystal Na system with 432 atoms and the length of each dimension of the supercell being 45.6 a.u., the total free energy evaluated using ABINIT is -103.27947 a.u.. Using the same setup as done in the crystal system with 4 EOs per atom, the total free energy evaluated using EO is -103.27588 a.u.. The difference is as small as 0.22 meV per atom. Since our implementation takes the spin-unpolarized form, we consider a system with two vacancies by removing 2 Na

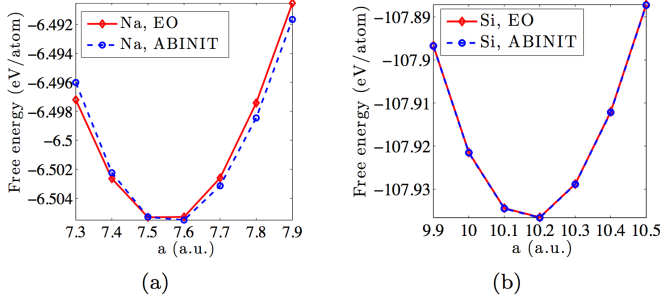


FIG. 5: (color online) The total free energy per atom for 3D bulk Na system with 432 atoms (a) and 3D bulk Si system with 512 atoms (b), with different lattice constants calculated from ABINIT (red line with diamonds) and from element orbitals (blue dashed line with circles).

atoms belonging to one unit cell from the supercell. All the parameters are the same as those for the calculation of the crystal system. The total free energy evaluated using ABINIT is -102.76957 a.u., and the total free energy evaluated using 4 EOs per atom is -102.76637 a.u., with the difference being 0.20 meV per atom. The error for both the crystal and the defect system is less than 1 meV per atom. We also estimate the formation energy of M neutral vacancies by

$$\Delta E(M) = E_{N-M}^d - E_N^0 \frac{N-M}{M}, \quad (12)$$

with E_N^0 being the free energy for the crystal system with N atoms, and E_{N-M}^d being the free energy for the same system but with M atoms removed. Atomic relaxation is not taken into account at this stage. Using (12), the formation energy calculated from ABINIT is 0.864 eV, and that calculated from EO is 0.854 eV. The difference of the formation energy is 0.010 eV, and the relative error of the formation energy is 1.2% .

The calculation of the defect formation energy for Si is as follows. For a crystal Si system with 512 atoms and the length of each dimension of the supercell being 40.4 a.u., the total free energy evaluated using ABINIT is -2030.85824 a.u., and the total free energy evaluated using 10 EOs per atom is -2030.85691 a.u.. The difference is as small as 0.07 meV per atom. A defect system is constructed by removing one Si atom, and all the parameters are the same as those for the crystal calculation. The total free energy evaluated using ABINIT is -2026.76478 a.u., and the total free energy evaluated using 10 EOs per atom is -2026.75974 a.u., with the difference being 0.27 meV per atom. The error for both the crystal system and that for the defect system is less than 1 meV per atom. The formation energy calculated from ABINIT is 3.454 eV, and that calculated from EO is 3.555 eV. The difference of the formation energy is 0.101 eV, and the relative error of the formation energy is 2.9% .

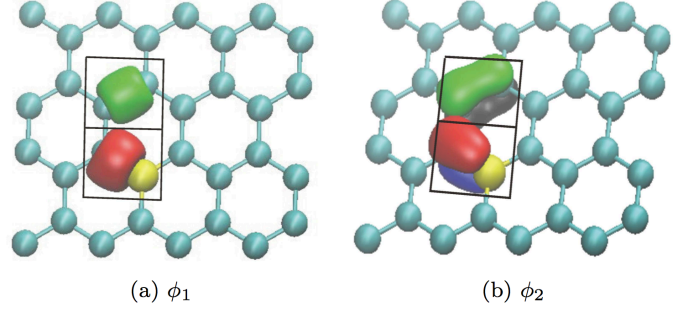


FIG. 6: Graphene sheet consisting of 32 C atoms (cyan balls) with 1 C atom substituted by a Si atom (gold ball). Each black box represents an element. (a) The first element orbital ϕ_1 (green) for the upper element with 2 C atoms, and the first element orbital ϕ_1 (red) for the lower element with 1 C atom and 1 Si atom. (b) The second element orbital ϕ_2 (green for the positive part and black for the negative part) for the upper element with 2 C atoms, and the second element orbital ϕ_2 (red for the positive part and blue for the negative part) for the lower element with 1 C atom and 1 Si atom.

Next we study graphene sheet consisting of 32 C atoms (cyan balls), with 1 C atom replaced by a Si atom (gold ball), as shown in Fig. 6. The length of the supercell is 10.000 a.u., 16.108 a.u. and 18.600 a.u. for x, y, z directions, respectively. The C and Si atoms are in the $y-z$ plane. The supercell consists of 4×4 elements, with each element containing 2 atoms, and represented by one black box. The length of each element is therefore 10.00 a.u., 4.027 a.u. and 4.650 a.u. along x, y, z directions, respectively. The shape of the EOs is shown in Fig. 6 (a) for the first EOs ϕ_1 belonging to 2 different elements, and (b) for the second EOs ϕ_2 belonging to the same 2 elements, respectively. We find that ϕ_1 in the upper element reflects the C-C bond and ϕ_1 in the lower element reflects the C-Si bond, respectively. Similarly, ϕ_2 reflects the π bonds in both the upper and the lower elements. The shape of the EOs agree well with the physical intuition. In particular, the element orbitals are not centered around individual atoms but correspond directly to chemical bonds, which are of lower energy than individual atomic orbitals. Fig. 6 shows that the EOs constructed from a complete basis set such as plane waves provides a more flexible treatment of chemical environment than atom centered orbitals. The total free energy calculated using ABINIT with a plane wave cutoff at 200 Ry is -180.56324 a.u.. 12 EOs per atom contracted from 40 ALBs per atom with localization radius being 3.0 a.u.. The total free energy calculated using EO is -180.56279 a.u.. The difference in the total free energy per atom is 0.38 meV.

A more complicated example is a graphene sheet with 512 C atoms, and with 128 of the C atoms randomly se-

lected and replaced by Si atoms. The atomic configuration is shown in Fig. 7 (a), with the C atoms represented by cyan balls and Si atoms represented by gold balls, respectively. The atoms are all in the $y-z$ plane, and the dimension of the supercell is 10.000 a.u., 64.432 a.u. and 74.400 a.u. along x, y, z directions, respectively. The electron density in the $y-z$ plane is shown in Fig. 7 (b). The total free energy calculated from ABINIT is -2639.02487 a.u., and the total free energy calculated from EO with 12 EOs per atom for all elements is -2639.11504 a.u.. The error of the total free energy per atom is 4.79 meV per atom.

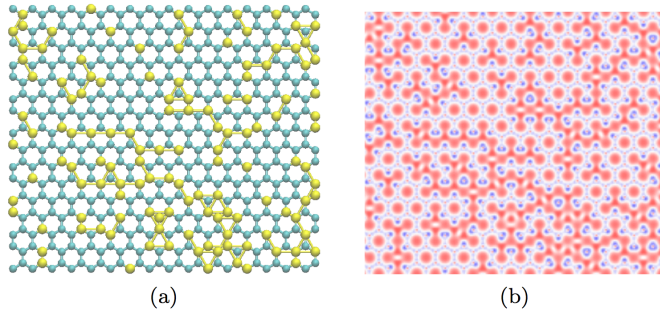


FIG. 7: (a) The atomic configuration of a graphene sheet consisting of 512 C atoms (cyan balls), with 128 C atoms randomly selected and substituted by Si atoms (gold balls). (b) The electron density across $y-z$ plane.

The fact that a small number of EOs per atom already achieve high accuracy allows us to perform calculations for systems of large size. Here we study 3D bulk Na systems of various sizes, ranging from 128 atoms to 4394 atoms. The length of the supercell along each dimension is also proportional to the system size, from 30.4 a.u. for 128 atoms to 98.8 a.u. for 4394 atoms. The number of processors (computational cores) used is chosen to be proportional to the number of atoms, with 64 processors used for 128 atoms, and 2196 processors used for 4392 atoms. 4 EOs per atom are constructed from 42 ALBs per atom for all calculations. The total time per SCF iteration is shown in Fig. 8. We find that even though the number of atoms increase by a factor of 34, the wall clock time only increases by less than 4 times from 114 sec for 128 atoms to 413 sec for 4394 atoms. The small increase of the total wall clock time is because the time for solving the generalized eigenvalue problem (10), which is asymptotically the computationally dominating part, only takes less than 100 sec even for system as large as 4392 atoms, thanks to the small number of basis functions per atom allowed to be used in the calculation. The time for generating the ALBs using LOBPCG and the time for constructing the EOs from the ALBs are flat for all systems, since these steps are localized in each extended element and the computational cost is independent of the global system size. The overall time for solving the generalized eigenvalue problem (10) has not dominated

the computational time for 4392 atoms with a Hamiltonian matrix of size 17568. However, the wall clock time for this part already scales quadratically with respect to the number of atoms. Since the number of processors scale linearly with respect to the system size, the overall time for solving the generalized eigenvalue problem scales cubically with respect to the system size, and will eventually dominate the overall running time for systems of larger size. The overhead of the DG calculation involves the assembly of the DG matrix H , the construction of the Hamiltonian matrix $C^t H C$ and the mass matrix $C^t C$ using parallel matrix-matrix multiplication, as well as the communication time. As alluded to earlier, the parallel matrix-matrix multiplication treats C and H as dense matrices in the current implementation. Therefore the asymptotic scaling of this part has the same asymptotic cubic scaling as solving the generalized eigenvalue problem. All the rest of the computational time (classified as “other time” in Fig. 8) mainly includes constructing the electron density using (11) in the global domain, solving the Kohn-Sham potential from the electron density, charge mixing as well as the extra data communication.

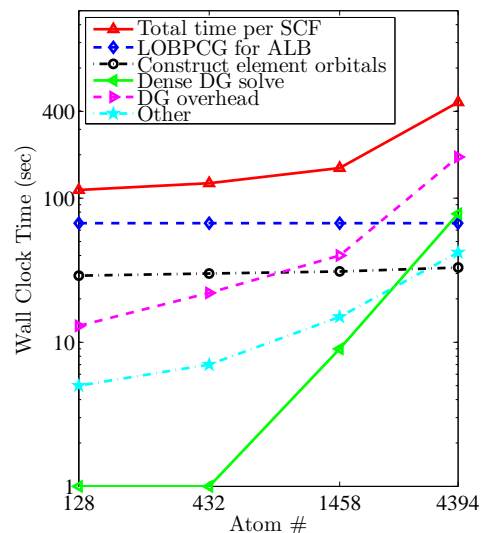


FIG. 8: (color online) The total computational time per SCF iteration (red solid line with upward-pointing triangles) for 3D bulk Na systems ranging from 128 atoms to 4394 atoms. The breakdown of the total computational time includes the time for using LOBPCG to generate adaptive local basis functions (blue dashed line with diamonds), the time for constructing the element orbitals from adaptive local basis functions (black dot dashed line with circles), the time for solving the generalized eigenvalue problem using dense ScaLAPACK solver (green solid line with left-pointing triangles), the overhead time for solving the DG problem (magenta dashed line with right-pointing triangles), and the rest of the time in a SCF iteration (cyan dot dashed line with stars).

We also remark that treating the Hamiltonian matrix as dense matrices greatly increases the memory cost and the communication volume. Fig. 9 (a) shows the amount of memory used per processor. When the number of atoms is 4394, the memory used per processor is 5.5 GB, which becomes the bottleneck for further increasing the system size, despite that the computational time per SCF is still within affordable range. The communication volume, indicated by the percentage of the communication time within the total computational time is shown in Fig. 9 (b). The communication time occupies more than 40% of the total time for systems with 4394 atoms. Both the large memory cost and the large communication volume is largely due to the treatment of C and H as dense matrices, and shall be improved in the future work.

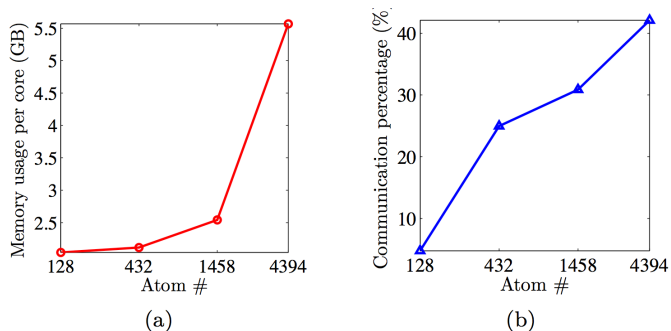


FIG. 9: (color online) The memory cost per processor (a) and the communication percentage (b) for 3D bulk Na systems ranging from 128 atoms to 4394 atoms.

VI. CONCLUSION

In conclusion, we have introduced the element orbitals for discretizing the Kohn-Sham Hamiltonian in the pseudopotential framework, which are contracted automatically from a uniform basis set. Comparing with the existing contracted basis sets, element orbitals incorporate environment information by including directly all atoms in the neighboring elements on the fly. The implementation of element orbitals is straightforward thanks to the rectangular partitioning of the domain. The accuracy of

element orbitals are systematically improvable and the same procedure can be applied to systems under various conditions. The element orbitals are constructed by solving KSDFT locally in the real space, and localized on each element via a localization procedure. We remark that the localization procedure used for constructing the element orbitals is not grounded on the near-sightedness property as in the linear scaling methods for insulating systems^{39,40}. Instead of finding the compact representations for the Kohn-Sham invariant subspaces⁴¹, the current work seeks for a set of compact basis functions in the real space, while the coefficients of the basis set for representing the Kohn-Sham orbitals can still be delocalized. As is shown by the numerical examples, the current procedure is applicable to both insulating and metallic systems.

Our numerical examples also indicate that treating C and H as dense matrices can greatly increase the memory cost, the communication volume and the computational time especially for systems of large size. The future improvement includes treating C and H as sparse matrices so that the construction of the Hamiltonian matrix $C^t H C$ and the mass matrix $C^t C$ is of linear scaling. By treating C and H as sparse matrices, we can also incorporate the recently developed pole expansion and selected inversion type fast algorithms^{25–30} to reduce the asymptotic scaling for solving the generalized eigenvalue problem (10) from cubic scaling to at most quadratic scaling for 3D bulk systems. We also remark that the current procedure for constructing the orbitals from adaptive local basis functions is still a costly procedure inside each element. Method for generating element orbitals directly inside the extended element is also under our exploration.

This work is partially supported by NSF CAREER Grant 0846501 (L. Y.), and by the Laboratory Directed Research and Development Program of Lawrence Berkeley National Laboratory under the U.S. Department of Energy contract number DE-AC02-05CH11231 (L. L.). The authors thank Jianfeng Lu for helpful discussions, and National Energy Research Scientific Computing Center (NERSC) for the support to perform the calculations. L. L. also thanks Weinan E for encouragement, and the University of Texas at Austin for the hospitality where the idea of this paper starts.

* Electronic address: linlin@lbl.gov

¹ W. Kohn and L. Sham, Phys. Rev. **140**, A1133 (1965).

² N. Troullier and J. L. Martins, Phys. Rev. B **43**, 1993 (1991).

³ D. Vanderbilt, Phys. Rev. B **41**, 7892 (1990).

⁴ O. K. Andersen, Phys. Rev. B **12**, 3060 (1975).

⁵ P. E. Blöchl, Phys. Rev. B **50**, 17953 (1994).

⁶ T. Ozaki, Phys. Rev. B **67**, 155108 (2003).

⁷ V. Blum, R. Gehrke, F. Hanke, P. Havu, V. Havu, X. Ren,

K. Reuter, and M. Scheffler, Comput. Phys. Commun. **180**, 2175 (2009).

⁸ J. Junquera, O. Paz, D. Sanchez-Portal, and E. Artacho, Phys. Rev. B **64**, 235111 (2001).

⁹ M. Chen, G. C. Guo, and L. He, J. Phys.: Condens. Matter **22**, 445501 (2010).

¹⁰ O. K. Andersen and T. Saha-Dasgupta, Phys. Rev. B **62**, R16219 (2000).

¹¹ X. Qian, J. Li, L. Qi, C. Z. Wang, T. L. Chan, Y. X. Yao,

- K. M. Ho, and S. Yip, Phys. Rev. B **78**, 245112 (2008).
- ¹² D. R. Bowler and T. Miyazaki, Rep. Prog. Phys. **75**, 036503 (2012).
 - ¹³ L. Lin, J. Lu, L. Ying, and W. E, J. Comput. Phys. **231**, 2140 (2012).
 - ¹⁴ D. N. Arnold, SIAM J. Numer. Anal. **19**, 742 (1982).
 - ¹⁵ X. Gonze, B. Amadon, P. M. Anglade, J. M. Beuken, F. Bottin, P. Boulanger, F. Bruneval, D. Caliste, R. Caracas, M. Cote, et al., Comput. Phys. Commun. **180**, 2582 (2009).
 - ¹⁶ M. J. Rayson and P. R. Briddon, Phys. Rev. B **80**, 205104 (2009).
 - ¹⁷ M. J. Rayson, Comput. Phys. Commun. **181**, 1051 (2010).
 - ¹⁸ N. Mermin, Phys. Rev. **137**, A1441 (1965).
 - ¹⁹ D. M. Ceperley and B. J. Alder, Phys. Rev. Lett. **45**, 566 (1980).
 - ²⁰ J. P. Perdew and A. Zunger, Phys. Rev. B **23**, 5048 (1981).
 - ²¹ L. Kleinman and D. M. Bylander, Phys. Rev. Lett. **48**, 1425 (1982).
 - ²² D. N. Arnold, F. Brezzi, B. Cockburn, and L. D. Marini, SIAM J. Numer. Anal. **39**, 1749 (2002).
 - ²³ Z. Zhao, J. Meza, and L. Wang, J. Phys.: Condens. Matter **20**, 294203 (2008).
 - ²⁴ C. J. García-Cervera, J. Lu, Y. Xuan, and W. E, Phys. Rev. B **79**, 115110 (2009).
 - ²⁵ L. Lin, J. Lu, R. Car, and W. E, Phys. Rev. B **79**, 115133 (2009).
 - ²⁶ L. Lin, J. Lu, L. Ying, and W. E, Chin. Ann. Math. Ser. B **30**, 729 (2009).
 - ²⁷ L. Lin, J. Lu, L. Ying, R. Car, and W. E, Commun. Math. Sci. **7**, 755 (2009).
 - ²⁸ L. Lin, C. Yang, J. Lu, L. Ying, and W. E, SIAM J. Sci. Comput. **33**, 1329 (2011).
 - ²⁹ L. Lin, C. Yang, J. Meza, J. Lu, L. Ying, and W. E, ACM. Trans. Math. Software **37**, 40 (2011).
 - ³⁰ L. Lin, M. Chen, C. Yang, and L. He, arxiv:1202.2159 (2012).
 - ³¹ A. Knyazev, SIAM J. Sci. Comp. **23**, 517 (2001).
 - ³² M. P. Teter, M. C. Payne, and D. C. Allan, Phys. Rev. B **40**, 12255 (1989).
 - ³³ L. S. Blackford, J. Choi, A. Cleary, E. D'Azevedo, J. Demmel, I. Dhillon, J. Dongarra, S. Hammarling, G. Henry, A. Petitet, et al., *ScaLAPACK Users' Guide* (SIAM, Philadelphia, PA, 1997).
 - ³⁴ C. Hartwigsen, S. Goedecker, and J. Hutter, Phys. Rev. B **58**, 3641 (1998).
 - ³⁵ J. E. Pask and P. A. Sterne, Phys. Rev. B **71**, 113101 (2005).
 - ³⁶ A. Alavi, J. Kohanoff, M. Parrinello, and D. Frenkel, Phys. Rev. Lett. **73**, 2599 (1994).
 - ³⁷ D. Anderson, J. Assoc. Comput. Mach. **12**, 547 (1965).
 - ³⁸ G. P. Kerker, Phys. Rev. B **23**, 3082 (1981).
 - ³⁹ S. Goedecker, Rev. Mod. Phys. **71**, 1085 (1999).
 - ⁴⁰ W. Kohn, Phys. Rev. Lett. **76**, 3168 (1996).
 - ⁴¹ F. Gygi, Phys. Rev. Lett. **102**, 166406 (2009).